Enhanced broadband Cherenkov second-harmonic generation in nonlinear photonic crystals with a spatial chirped pulse

Bufan Jin,[1,2] Xuemei Wu,[1,3] Weimin Shen,[4,5] and Zhi Hong Hang[1,2,3,*]

[1]*School of Physical Science and Technology and Collaborative Innovation Center of Suzhou Nano Science and Technology, Soochow University, Suzhou 215006, China*

[2]*Institute for Advanced Study, Soochow University, Suzhou 215006, China*

[3]*Jiangsu Key Laboratory of Frontier Material Physics and Devices, Suzhou 215006, China*

[4]*Key Lab of Modern Optical Technologies of Education Ministry of China, School of Optoelectronic Science and Engineering, Soochow University, Suzhou 215006, China*

[5]*Key Lab of Advanced Optical Manufacturing Technologies of Jiangsu Province, School of Optoelectronic Science and Engineering, Soochow University, Suzhou 215006, China*

(Received 24 January 2024; revised 19 April 2024; accepted 24 April 2024; published 10 May 2024)

In this work, we theoretically study the role of the spatial chirped pulse in the Cherenkov second-harmonic generation in one-dimensional nonlinear photonic crystals. We show that the spatial chirped input with narrower spectral peaks but wider angular distribution can be used to cancel the natural dispersion of crystals, fitting the phase-matching condition at wider emission angles. Contrary to popular belief, the phase-matching bandwidth can remain almost unchanged with the growth of interaction length, leading to a substantial increase in the signal strength and bandwidth under long interaction. The improvement ratio of the signal can be as high as needed, if the beam waist and the interaction length are large enough.

DOI: 10.1103/PhysRevA.109.053513

I. INTRODUCTION

As an important branch of nonlinear optics, second-harmonic generation in nonlinear photonic crystals [1] has attracted a lot of research interest [2–10], where phase matching is a vital issue to be conquered [11]. In order to satisfy the longitudinal phase-matching conditions, the signal wave shall emit into an oblique direction [12], whose behavior bears a certain similarity to the Cherenkov radiation. The transverse phase matching can be achieved with the help of a one-dimensional (1D) photonic crystal design [13], whose nonlinear susceptibility index is periodically modulated. In order to build up a strong nonlinear signal, long interaction lengths are usually needed, as the signal power grows quadratically with the interaction distance when phase matching is satisfied. However, a phase-matching bandwidth usually decreases with the growth of interaction length. The decreasing angular distribution limits the efficient growth of the signal under long interaction length, which cannot be easily overcome with structural design or by manipulating material properties. To solve the problem, as the nonlinear effect is directly related to the field distribution of incident pulse, it is wise to control the nonlinear signal with the structured incident pulse combining with the structured media [14]. Though spatial-temporal distortions in structured light are common and often considered harmful, as they usually increase the pulse duration and reduce the peak laser intensity, with advanced control degrees [15–18], the spatial-temporal coupling can also be extremely advantageous. Thanks to the rapid growth of light modulation technology, it is possible to control all the beam's degrees of freedom and dimensions [19].

Here, through theoretical analysis and numerical simulations, we show that with the input pulse of suitable angular dispersion, second-harmonic generation in nonlinear photonic crystals can be greatly enhanced. The physics underneath is found that the chirped beam with different frequency components propagating in different directions can fit the phase-matching condition at wider incident angles, broadening the phase-matching bandwidth under large interaction length.

II. THEORETICAL ANALYSIS

We start from the nonlinear wave equation in frequency domain. As the nonlinear signal is normally very weak, we can ignore its source term in the wave equation of the fundamental pulse $\hat{E}_1$, thus the coupling wave equation [20] under paraxial condition becomes

$$\frac{\partial \hat{E}_1}{\partial z} + in_1(\omega_1)k_1\hat{E}_1 + \frac{i}{2n_1(\omega_1)k_1}\nabla^2\hat{E}_1 = 0,$$
$$\frac{\partial \hat{E}_2}{\partial z} + in_2(\omega_2)k_2\hat{E}_2 + \frac{i}{2n_2(\omega_2)k_2}\nabla^2\hat{E}_2 = \frac{i\omega_2^2 d}{n_2(\omega_2)k_2 c}\hat{E}_1^2, \quad (1)$$

where ω is the working frequency, c is the speed of light in free space, $k = \omega/c$ is the wave vector in free space, d is the nonlinear susceptibility, and $n(\omega)$ is the frequency-dependent refractive index, which can be calculated using the Sellmeier

*zhhang@suda.edu.cn

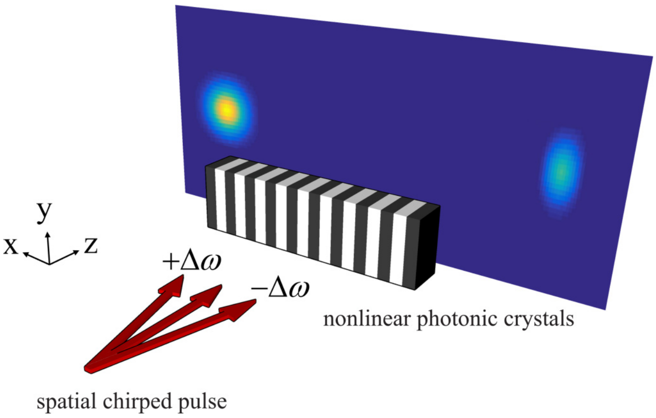

FIG. 1. The scenario considered. A spatial chirped pulse enters the nonlinear photonic crystals, generating the second-harmonic signal in the Cherenkov angle. The sign of nonlinear susceptibility varies periodically along the x direction, and the spatial chirped pulse propagates along the z direction.

equation [21,22]. The subscripts 1 and 2 correspond to the fundamental wave and the second harmonic, respectively.

We consider the scenario of a spatial chirped pulse passing through the 1D photonic crystals as shown in Fig. 1. The light beam is propagating along the z direction and the nonlinear susceptibility $d = d_{\text{eff}}g(x)$ is spatially modulated along the x direction with the period Λ. The modulation function is

$$g(x) = \begin{cases} 1, & m\Lambda < x < m\Lambda + 0.5\Lambda, \\ -1, & m\Lambda + 0.5\Lambda < x < m\Lambda + \Lambda, \end{cases} \tag{2}$$

which can be expanded with Fourier series

$$g(x) = \sum_m c_m \exp\left(-im\frac{2\pi}{\Lambda}x\right). \tag{3}$$

The spatial chirped input takes the following form [23]:

$$\begin{aligned} \hat{E}_1(\omega, x, y, z) = f(\omega)&\frac{1}{w_0(1-iz/z_0)}\exp(-ikz) \\ &\times \exp\left[\frac{ikz}{2(1-iz/z_0)}\left(\frac{x}{z} - \beta\Delta\omega\right)^2 - ik\frac{x^2}{2z}\right] \\ &\times \exp\left[-\frac{y^2}{w_0^2(1-iz/z_0)}\right], \end{aligned} \tag{4}$$

where $\Delta\omega = \omega - \omega_0$ is the deviation from the central frequency ω_0, $f(\omega) = \sqrt{\tau_0}\exp[-\Delta\omega^2\tau_0^2c^2/4]$ is the Gaussian spectral profile, w_0 is the beam waist and $z_0 = 0.5kw_0^2$ is the Rayleigh length. From the standpoint of the construction of a structured pulse, the spatial chirped pulse is the superposition of different frequency components ω traveling in different directions θ_1 in the XZ plane, with an extra angular dispersion $\beta = \partial\theta_1/\partial\omega$ compared with a normal Gaussian pulse. Such a spatial chirped pulse can be generated from a prism pair, tilted substrate, or $f-f$ Fourier-synthesis pulse shaper [24]. Considering the input pulse entering the photonic crystal at $z = 0$, the fundamental field in the crystal takes the identical form as Eq. (4) by replacing $k \to n_1k$.

In this Cherenkov second-harmonic generation process, the signal shall emit in the oblique direction to satisfy the longitudinal phase-matching condition. For the initial wave vector $n_1k(\sin\theta_1\cos\varphi_1, \sin\theta_1\sin\varphi_1, \cos\theta_1)$ and second-harmonic wave vector $2n_2k(\sin\theta_2\cos\varphi_2, \sin\theta_2\sin\varphi_2, \cos\theta_2)$, the corresponding transverse $(\Delta k_x, \Delta k_y)$ and longitudinal (Δk_z) phase mismatch can be described as

$$\begin{aligned} \Delta k_x &= 2kn_2\sin\theta_2\cos\varphi_2 - 2m\frac{\pi}{\Lambda} - 2kn_1\sin\theta_1\cos\varphi_1, \\ \Delta k_y &= 2kn_2\sin\theta_2\sin\varphi_2 - 2kn_1\sin\theta_1\sin\varphi_1, \\ \Delta k_z &= 2kn_2\cos\theta_2 - 2kn_1\cos\theta_1, \end{aligned} \tag{5}$$

which can be expanded in terms of a Taylor series around ω_0,

$$\Delta k(\omega) = \Delta k(\omega_0) + \left.\frac{\partial(\Delta k)}{\partial\omega}\right|_{\omega_0}\Delta\omega + \ldots. \tag{6}$$

For the finite interaction length L, a mismatch $\Delta kL \sim \pi$ is allowed. In order to get a broad phase-matching bandwidth,$\partial(\Delta k)/\partial\omega = 0$ is required. In this way the phase-matching bandwidth $\sim\Delta\omega$ will be irrelevant with the interaction length L, so that the signal can grow efficiently even under long interaction length. From Eq. (5), it requires that

$$\begin{aligned} &\frac{\partial(kn_2)}{\partial\omega} - \frac{\partial(kn_1)}{\partial\omega}[\sin\theta_1\sin\theta_2\cos(\varphi_1-\varphi_2) + \cos\theta_1\cos\theta_2] \\ &- kn_1\frac{\partial(\theta_1)}{\partial\omega}[\cos\theta_1\sin\theta_2\cos(\varphi_1-\varphi_2) - \sin\theta_1\cos\theta_2] = 0. \end{aligned} \tag{7}$$

It can be seen that, if using nonchirped input $\partial\theta_1/\partial\omega = 0$, it is not always possible to satisfy this condition. As the range of sine and cosine functions is $[-1, 1]$, Eq. (7) has no solution when $\partial(kn_2)/\partial\omega > \partial(kn_1)/\partial\omega$. On the contrary, when using the chirped input, with the new freedom $\beta = \partial\theta_1/\partial\omega \neq 0$ we can always find the solution of Eq. (7).

Here, we consider phase matching is perfectly satisfied for the first diffraction $m = \pm 1$ emitting at $\pm\theta_0$ by the central frequency ω_0 with wave vector k_0 propagating along $\theta_1 = 0$, i.e.,

$$\begin{aligned} \Delta k_x &= 2k_0n_2(2\omega_0)\sin\theta_0\cos\varphi_2 - \frac{2\pi}{\Lambda} = 0, \\ \Delta k_y &= 2k_0\sin\theta_0\sin\varphi_2 = 0, \\ \Delta k_z &= 2k_0n_2(2\omega_0)\cos\theta_0 - 2k_0n_1(\omega_0) = 0. \end{aligned} \tag{8}$$

It can be seen that the transverse phase-matching direction is accomplished through the reciprocal lattice vector. Since there is no reciprocal lattice vector along the y direction, it yields $\varphi_2 = 0$ and the generated pattern exhibits as a pair of spots as shown in Fig. 1. It is noted that by replacing $m = 1 \to m = -1$ and $\theta_0 \to -\theta_0$, the form of Eq. (7) is not identical, so that the spots are not symmetrical.

By factoring out the propagation coordinate from the electric field $\hat{E}(\omega) = \hat{A}(\omega)\exp(-inkz)$, Eq. (1) can be solved with the help of Fourier transform $\mathcal{F}[\hat{E}](z, k_x, k_y) = \int\int\hat{E}(z, x, y)\exp(-ik_xx - ik_yy)dx\,dy$.

Under paraxial limitation the second derivative term can be neglected, thus the second-harmonic signal $\hat{E}_2$ emitting at $\theta_2 = \sqrt{k_x^2 + k_y^2}/(n_2k_2)$, $\varphi = \arctan(k_y/k_x)$ can be written as

$$\hat{E}_2(2\omega,\theta_2,\varphi,z) = \sum_m \left(c_m \frac{2ikd}{n_2} f_2(\omega) \exp\left[-i2kn_2\left(1+\frac{\theta_2^2}{2}\right)z\right] \exp\left\{-w_0^2\left[\left(kn_2\sin\theta_2\cos\varphi - kn_1\beta\Delta\omega - m\frac{\pi}{\Lambda}\right)^2 + (kn_2\sin\theta_2\sin\varphi)^2\right]\Big/2\right\} \times \int_0^z \frac{\pi}{2[1+i(z'/z_0n_1)]} \exp\{-i[2kn_2\cos\theta_2 - 2kn_1]z'\} \times \exp\left\{-i\left[\left(kn_2\sin\theta_2\cos\varphi - m\frac{\pi}{\Lambda}\right)^2 + (kn_2\sin\theta_2\sin\varphi)^2\right]z'\Big/(kn_1)\right\}dz'\right), \tag{9}$$

Here, the spectral function $f_2(\omega) = \exp[-\Delta\omega^2\tau_0^2/2]$ and transverse envelope take the Gaussian form. In the following, we only consider the first diffraction $m = \pm 1$ corresponding to the signal emitting around $\pm\theta_0$, as the signal in other directions suffers destructive interference. As the spectral-dependent term $kn_1(\omega)\beta\Delta\omega$ is involved in the spatial envelopes, we can rewrite the two exponential functions in Eq. (9) with frequency gradient. For simplicity we set $\varphi = 0$, which yields

$$\begin{aligned}&\exp\big\{-w_0^2[kn_2(2\omega)\sin\theta_2 - kn_1(\omega)\beta\Delta\omega - k_0n_2(2\omega_0)\sin\theta_0]^2/2\big\}f_2(\omega)\\ &= \exp\big\{-w_2^2[kn_2(2\omega)\sin\theta_2 - k_0n_2(2\omega_0)\sin\theta_0]^2/2\big\}\\ &\quad\times\exp\big(-\tau_2^2\{\alpha[kn_2(2\omega)\sin\theta_2 - k_0n_2(2\omega_0)\sin\theta_0] - n_1(\omega)\Delta\omega\}^2/2\big),\end{aligned} \tag{10}$$

where $\alpha = kw_0^2\beta/\tau_2^2$ is the frequency gradient, $w_2 = \sqrt{w_0^2 - \tau_2^2\alpha^2}$ is the modified beam waist, and $1/\tau_2 = 1/\sqrt{k^2w_0^2\beta^2 + \tau_0^2/n_1^2}$ is the modified frequency bandwidth. When using the input with large waist and small temporal length $w_0 \gg \tau_0 c$, it leads to $w_2 \approx \tau_0\alpha/n_1$, $\tau_2 \approx w_0/\alpha$, where the status of waist w and temporal length τ exchanges. This means that compared with the nonchirped case, the signal consists of many narrow spectra $1/\tau_2 < 1/\tau_0$ so that the peak intensity is decreased, but the signal's angular distribution $1/(kw_2) > 1/(kw_0)$ is greatly broadened. The central frequency at different position θ satisfies

$$\alpha[kn_2(2\omega)\sin\theta - k_0n_2(2\omega_0)\sin\theta_0] - n_1(\omega)\Delta\omega = 0. \tag{11}$$

III. RESULTS

We take photonic crystals made of lithium niobate [25] as an example, which is one of the most popular materials for nanoengineering. Its wavelength-dependent refractive indices can be calculated using the Sellmeier equation [21,22]. We consider the type-I phase-matching (oo-e) and set the central wavelength of the incident beam in free space being 0.8 μm. From Eq. (7) we get the required chirp factor $\beta_1 = 0.41$ fs. It is noticed that with these parameters, it is derived that $\partial(kn_2)/\partial\omega > \partial(kn_1)/\partial\omega$, so that the phase matching cannot be obtained by only adjusting the incident angle if using the nonchirped input.

In Fig. 2, we provide the spectrum of the signal at different emitting angles θ, where we set $\varphi = 0$ for simplicity. We use the chirped pulse in Figs. 2(c)–2(f), and the nonchirped pulse in Figs. 2(a) and 2(b) for comparison. In the nonchirped case the spectrum around $\pm\theta_0$ is identical, while in the chirped case the spectrum is different between θ_0 [Figs. 2(c) and 2(d)] and $-\theta_0$ [Figs. 2(e) and 2(f)]. As an example, we set $w_0 = 60$ μm, $\tau_0 = 25$ fs, and the corresponding parameters are $w_2 \approx \tau_0\alpha/n_1 = 3.3$ μm, $\tau_2 \approx w_0/\alpha = 200$ fs. For an infinite short interaction length [Figs. 2(a), 2(c), and 2(e)], the acceptance bandwidth is infinite and only the transverse phase matching needs to be considered. It can be seen that the signal's spectra are greatly changed by the chirp parameter, exhibiting wider angular distribution around θ_0 and narrower spectral peaks at different emitting angles (red line). In the meantime, the total spectrum around θ_0 (blue dashed line) in both cases remains the same. However, for long interaction length $0.02z_0$ [Figs. 2(b), 2(d), and 2(f)], longitudinal phase matching is vital. In the nonchirped case the signal can only be efficiently generated in a small range around $\pm\theta_0$, and the corresponding total spectrum bandwidth $\sim 1/w_0$ (blue dashed line) is very narrow. On the contrary, in our proposed chirped signal incidence scenario, phase matching can be satisfied in a wider range around θ_0, so that the pulse's energy at the larger divergence angle can still be made use of, leading to a large numerical aperture and broad bandwidth. The total spectrum $\sim 1/w_2$ is almost irrelevant with z, so that around θ_0 we can estimate the incremental rate being w_0/w_2 from the integrations

$$\int_{-\infty}^{\infty} \exp(-ax^2)dx = \sqrt{\pi/a}. \tag{12}$$

The signal around $-\theta_0$, however, decays even faster than the nonchirped case owing to the wrong sign of the chirp factor, with the spectrum bandwidth $\sim 1/(2w_0)$, so that we can estimate the total incremental rate of the two cases being $(w_0 + w_2)/(2w_2)$, as the results can be found in Fig. 3.

In Fig. 3, we depict the ratio of generated photons with a chirped pulse to that with a nonchirped pulse, as the function of interaction length. For an interaction length of 1mm, an improvement ratio of 7 can be obtained. The result can be well explained by the above analysis: Under small interaction length, the improvement ratio grows quickly, because in the chirped case phase matching is perfectly satisfied, while in the nonchirped case the acceptance bandwidth quickly drops

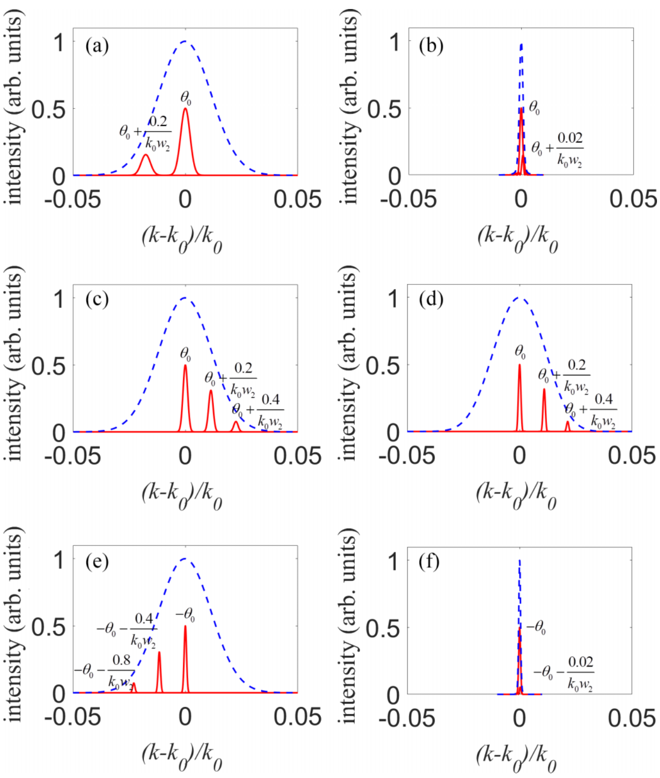

FIG. 2. The normalized signal spectrum for nonchirped input (a),(b) and chirped input (c),(d) with $\beta = 0.41$ fs, $w_0 = 60\,\mu\text{m}$, and $\tau_0 = 25\,\text{fs}$. The red line refers to the spectrum at different angles (from left to right): (a) $\theta_0 + 0.2/(k_0w_2), \theta_0$; (b) $\theta_0, \theta_0 + 0.02/(k_0w_2)$; (c) $\theta_0, \theta_0 + 0.2/(k_0w_2), \theta_0 + 0.4/(k_0w_2)$; (d) $\theta_0,\ \theta_0 + 0.2/(k_0w_2), \theta_0 + 0.4/(k_0w_2)$; (e) $-\theta_0 - 0.8/(k_0w_2), -\theta_0 - 0.4/(k_0w_2), -\theta_0$; (f) $-\theta_0, -\theta_0 - 0.02/(k_0w_2)$; and the blue dashed line refers to the total spectrum at all angles. The interaction length is $10^{-7}z_0$ in (a), (c), and (e) and is $0.02z_0$ in (b), (d), and (f).

to $\sim 1/w_0$. Under long interaction length, the ratio stops growing, because the allowed longitudinal phase mismatch $\sim \pi/z$ in both cases is the same, both decreasing with the growth of the interaction length and phase matching is quasisatisfied. Therefore, if the spectrum bandwidth at a certain angle in Fig. 2(c) is initially narrow enough, i.e., the beam waist is

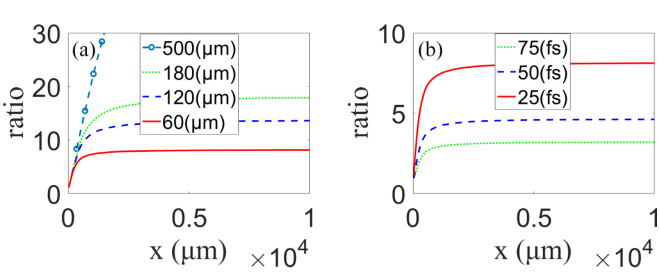

FIG. 3. The improvement ratio of the generated photon by chirped pulse to that of the nonchirped case as the function of interaction length, with (a) $\beta = 0.41$ fsand $\tau_0 = 25\,\text{fs}$ and different focus waists $w_0 = 60,\ 120,\ 180$, and $500\,\mu\text{m}$ and (b) $\beta = 0.41$ fs, $w_0 = 60\,\mu\text{m}$ and different temporal lengths $\tau_0 = 25$, 50, and 75 fs. For the case $w_0 = 500\,\mu\text{m}$ the second chirped parameter $\beta_2 = 0.28\ \text{fs}^2$ is used.

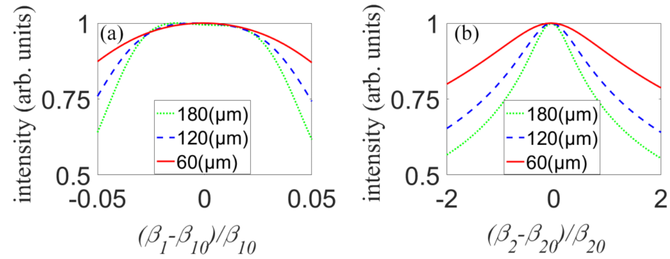

FIG. 4. The normalized intensity of the signal generated by chirped pulse $\beta_{10} = 0.41$ fs and $\beta_{20} = 0.28\ \text{fs}^2$ with different waists $w_0 = 60,\ 120,$ and $180\,\mu\text{m}$, under (a) different first-order chirp parameters β_1, and (b) different second-order chirp parameters β_2.

large enough, even for a long interaction length the phase matching can still be perfectly satisfied, so that the improvement ratio can be as high as needed.

It is noticed that for the small waist $w_0 = 60\,\mu\text{m}$, the incremental ratio is close to the predicted number $(w_0 + w_2)/(2w_2) = 9.5$, while for large w_0 the ratio is deviated from that. This is because the first-order chirp parameter β_1 does not perfectly fit the crystals' dispersion, while the larger waist with narrower spectrum peaks strongly depends on the precise location of the phase matching. As shown in Fig. 4(a), for $w_0 = 180\,\mu\text{m}$, the signal does not reach its maximum when $\beta_1 = \beta_{10} = 0.41$ fs, which means higher-order parameters have to be considered. It can be seen in Fig. 4(b) that the second-order chirped parameters strongly influence the results for large waist. When the second-order chirp $\beta_2 = \beta_{20} = 0.5\partial^2\theta_1/\partial\omega^2 = 0.28\ \text{fs}^2$ is considered [by replacing $\beta\Delta\omega \rightarrow \beta_1\Delta\omega + \beta_2(\Delta\omega)^2$ in Eq. (4)], the signal can grow efficiently in a wide range. As manifested in Fig. 3(a), at a large beam waist $w_0 = 500\ \mu$m, the improvement ratio can be up to 30 for $z = 1.5$ mm.

Large w_0 and small τ_0 is beneficial to not only the improvement ratio but also the signal strength. As the second-harmonic signal has a quadratic relationship with the incident beam's intensity, it is superior to choose a smaller pulse duration. For different beam waist, though smaller w_0 corresponds to a larger intensity within the beam's Rayleigh length z_0, the pulse's intensity drops quickly at the position exceeding z_0, and the larger waist with larger Rayleigh length takes more

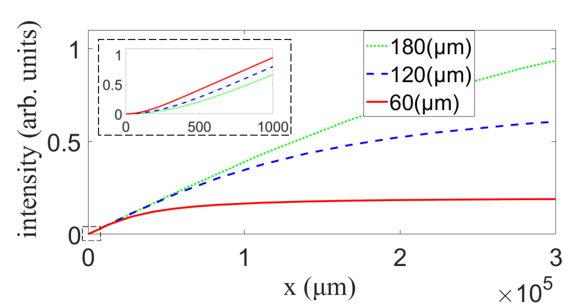

FIG. 5. The normalized intensity of the signal generated by the chirped pulse as the function of interaction length, with $\beta = 0.41$ fs, $\beta_{20} = 0.28\ \text{fs}^2$, and $\tau_0 = 25\,\text{fs}$ and different focus waists $w_0 = 60,\ 120,$ and $180\,\mu\text{m}$. The inset depicts the details of the signal under small interaction length.

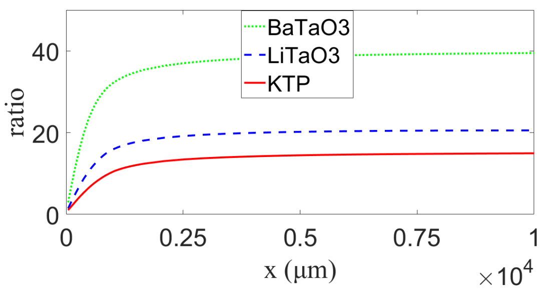

FIG. 6. The ratio of the generated photon by chirped pulse to that of the nonchirped case as the function of interaction length with $\lambda = 0.8\,\mu\text{m}$, $w_0 = 180\,\mu\text{m}$, and $\tau_0 = 25$ fs and different chirped parameters for $LiTaO_3$, $BaTiO_3$, and KTP. The Sellmeier equations are from [26–28].

advantage. As shown in Fig. 5, when interaction length z is small, phase match is perfectly satisfied, and the signal has a quadratic relationship with the interaction length. When the single spectral peak's bandwidth $1/w_0$ exceeds the allowed longitudinal phase mismatch π/z, the phase is quasimatched, and the signal has a linear relationship with the interaction length. When the interaction length exceeds the Rayleigh length, the signal grows slower and the larger w_0 is superior. Thus, the signal grows steadily for a wide range of z from 0 to several times the Rayleigh length, which makes using longer crystals worthwhile.

IV. DISCUSSION

In practice, our proposal is effective to other materials considered and other structures with spatially modulated nonlinearity as well, such as other periodically poled ferroelectric materials. Starting from the wavelength-dependent refractive indices, we can adjust the signal's angle-dependent spectrum [Eq. (11)] by fitting the phase-matching requirement in Eqs. (5) and (7) with different β. As an example, in Fig. 6, we give the improvement ratio of generated photons with a chirped pulse to that with a nonchirped pulse as the function of the interaction length for periodically modulated $LiTaO_3$, $BaTiO_3$, and $KTiOPO_4$ (KTP). We set the parameters of the incident pulse as $\lambda = 0.8\,\mu\text{m}$, $w_0 = 180\,\mu\text{m}$, and $\tau_0 = 25$ fs with different chirp factors for different crystals. The detailed parameters can be seen in Table I. For $LiTaO_3$ and $BaTiO_3$, we consider the type-I phase-matching (oo-e). For KTP we consider the similar situation in [13], where the fundamental beam propagating along the crystals' polar axis (z) is y polarized and the second-harmonic generation is x polarized. The spatial chirped pulse greatly increases the signal, and the varying trends of the ratio are similar with $LiNbO_3$.

TABLE I. Beam and crystals parameters.

Material	Λ (μm)	θ_0 (deg)	β_1 (fs)	β_2 (fs^2)	w_0/w_2
$BaTiO_3$	0.65	24.35	0.62	0.54	82.88
$LiTaO_3$	0.52	19.14	0.35	0.17	42.89
KTP	0.78	15.97	0.31	0.16	30.35

In experiments, the higher-order chirped parameters required by the larger waist can be realized with the help of metasurfaces [29]. The output signal inherits the chirp characteristic $\beta n_1/n_2$ of the input pulse and can be converted back into the nonchirped pulse with a similar optical system.

Furthermore, our proposal has the potential to enhance other nonlinear processes that require both long interaction and broad bandwidth. For example, in the head-on collision of a chirped probe laser k_p and a background laser k_b, the latter should have a much larger temporal length and can be viewed as monochromatic light in order to get a larger interaction length. The differential of phase-matching equations leads to ($\varphi = 0$ for simplicity)

$$\frac{\partial(k_s n_s)}{\partial\omega} - \frac{\partial(k_p n_p)}{\partial\omega}\cos\theta_s - k_p n_p \beta \sin\theta_s = 0. \tag{13}$$

Following similar steps, we can adjust β to fit this condition so that the wave-mixing signal k_s can be efficiently generated. In summary, the angle-dependent spectrum breaks the limitation of the narrow phase-matching bandwidth of the long interaction length, so that the signal's strong intensity and broad bandwidth can be obtained at the same time.

V. CONCLUSION

We investigate the Cherenkov second-harmonic generation in the 1D photonic crystals $LiNbO_3$, $LiTaO_3$, $BaTiO_3$, and KTP, estimating an enhancement as high as needed if the beam waist and interaction length are large enough. We provide a general recipe to enhance the nonlinear signal with a spatial chirped pulse input. The spectrum bandwidth and divergence angle of the signal can remain almost unchanged with the growth of the interaction length, and the intensity of the signal can be greatly enhanced when using the input pulse with a large waist and small temporal length.

ACKNOWLEDGMENTS

This work was supported by National Natural Science Foundation of China (Grant No. 12274315), National Key R&D Program of China (Grant No. 2022YFA1404400), a project funded by the Priority Academic Program Development of Jiangsu Higher Education Institutions (PAPD), and Jiangsu Funding Program for Excellent Postdoctoral Talent (Grant No. 2023ZB537).

[1] V. Berger, Phys. Rev. Lett. **81**, 4136 (1998).
[2] N. G. R. Broderick, G. W. Ross, H. L. Offerhaus, D. J. Richardson, and D. C. Hanna, Phys. Rev. Lett. **84**, 4345 (2000).
[3] K. Kalinowski, P. Roedig, Y. Sheng, M. Ayoub, J. Imbrock, C. Denz, and W. Krolikowski, Opt. Lett. **37**, 1832 (2012).
[4] A. M. Vyunishev, V. V. Slabko, I. S. Baturin, A. R. Akhmatkhanov, and V. Ya. Shur, Opt. Lett. **39**, 4231 (2014).

[5] H. Liu, J. Li, X. Zhao, Y. Zheng, and X. Chen, Opt. Express **24**, 15666 (2016).

[6] X. Fang, H. Wang, H. Yang, Z. Ye, Y. Wang, Y. Zhang, X. Hu, S. Zhu, and M. Xiao, Phys. Rev. A **102**, 043506 (2020).

[7] S. Liu, L. Wang, L. M. Mazur, K. Switkowski, B. Wang, F. Chen, A. Arie, W. Krolikowski, and Yan Sheng, Adv. Opt. Mater. **11**, 2300021 (2023).

[8] H. Liu, H. Li, Y. Zheng, and X. Chen, Opt. Lett. **43**, 5981 (2018).

[9] N. V. Bloch, K. Shemer, A. Shapira, R. Shiloh, I. Juwiler, and A. Arie, Phys. Rev. Lett. **108**, 233902 (2012).

[10] L. Hong, B. Chen, C. Hu, P. He, and Z. Y. Li, Phys. Rev. Appl. **18**, 044063 (2022).

[11] J. A. Armstrong, N. Bloembergen, J. Ducuing, and P. S. Pershan, Phys. Rev. **127**, 1918 (1962).

[12] V. Vaicaitis, Opt. Commun. **209**, 485 (2002).

[13] A. Fragemann, V. Pasiskevicius, and F. Laurell, Appl. Phys. Lett. **85**, 375 (2004).

[14] W. T. Buono and A. Forbes, Opto-Electron. Adv. **5**, 210174 (2022).

[15] G. Pariente, V. Gallet, A. Borot, O. Gobert, and F. Quéré, Nat. Photonics **10**, 547 (2016).

[16] A. Sainte-Marie, O. Gobert, and F. Quere, Optica **4**, 1298 (2017).

[17] H. Vincenti and F. Quéré, Phys. Rev. Lett. **108**, 113904 (2012).

[18] Dustin H. Froula, David Turnbull, Andrew S. Davies, Terrance J. Kessler, Dan Haberberger, John P. Palastro, Seung-Whan Bahk, Ildar A. Begishev, Robert Boni, Sara Bucht *et al.*, Nat. Photonics **12**, 262 (2018).

[19] A. Forbes, M. de Oliveira, and M. R. Dennis, Nat. Photonics **15**, 253 (2021).

[20] R. W. Boyd, A. L. Gaeta, and E. Giese, *Nonlinear Optics*, 3rd ed. (Academic, New York, 2008).

[21] D. H. Jundt, Opt. Lett. **22**, 1553 (1997).

[22] G. Edwards and M. Lawrence, Opt. Quantum Electron. **16**, 373 (1984).

[23] S. Akturk, X. Gu, E. Zeek, and R. Trebino, Opt. Express **12**, 4399 (2004).

[24] X. Gu, S. Akturk, and R. Trebino, Opt. Commun. **242**, 599 (2004).

[25] R. Weis and T. Gaylord, Appl. Phys. A **37**, 191 (1985).

[26] M. Nakamura, S. Higuchi, S. Takekawa, K. Terabe, Y. Furukawa, and K. Kitamura, Jpn. J. Appl. Phys. **41**, L465 (2002).

[27] K. Buse, S. Riehmann, S. Loheide, H. Hesse, F. Mersch, and E. Krätzig, Phys. Status Solidi A **135**, K87 (1993).

[28] H. Zhou, X. He, W. Wu, J. Tong, J. Wang, Y. Zuo, Y. Wu, C. Zhang, and Z. Hu, Light Sci. Appl. **12**, 23 (2023).

[29] X. Zhang, Q. Li, F. Liu, M. Qiu, S. Sun, Q. He, and L. Zhou, Light Sci. Appl. **9**, 76 (2020).